Acta Crystallographica Section B
Structural Science
ISSN 0108-7681

Mode-crystallography analysis and magnetic structures of $SrLnFeRuO_6$ (*Ln* = La, Pr, Nd) disordered perovskites

E. Iturbe-Zabalo,[a,b]* O. Fabelo,[c,b] M. Gateshki[d] and J. M. Igartua[a]

[a]Fisika Aplikatua II Saila, Zientzia eta Teknologia Fakultatea, UPV/EHU, PO Box 644, 48080 Bilbao, Spain, [b]Institut Laue–Langevin (ILL), 6 rue Jules Horowitz, BP156, 38042 Grenoble CEDEX 9, France, [c]Instituto de Ciencia de Materiales de Aragón, CSIC-Universidad de Zaragoza, 50009 Zaragoza, Spain, and [d]PANalytical, BV PO Box 13, 7600 AA Almelo, The Netherlands

Correspondence e-mail: edurne.iturbe@ehu.es

Received 26 July 2012
Accepted 24 October 2012

The crystal and magnetic structures of $SrLnFeRuO_6$ (*Ln* = La, Pr, Nd) double perovskites have been investigated. All compounds crystallize with an orthorhombic *Pbnm* structure at room temperature. These materials show complete chemical disorder of Fe and Ru cations for all compounds. The distortion of the structure, relative to the ideal cubic perovskite, has been decomposed into distortion modes. It has been found that the primary modes of the distortion are octahedral tilting modes: R_4^+ and M_3^+. The crystal structure of $SrPrFeRuO_6$ has been studied from room temperature up to 1200 K by neutron powder diffraction. There is a structural phase transition from orthorhombic (space group *Pbnm*) to trigonal (space group $R\bar{3}c$) at T = 1075 K. According to group theory no second-order transition is possible between these symmetries. Magnetic ordering for all the compounds is described by the magnetic propagation vector (0,0,0). $SrPrFeRuO_6$ shows ferrimagnetic order below *ca* 475 K, while $SrLaFeRuO_6$ (below *ca* 450 K) and $SrNdFeRuO_6$ (below *ca* 430 K) exhibit canted-antiferromagnetic order. The magnetic moments at low temperatures are m(Fe/Ru) = 1.88 (3)μ_B for $SrLaFeRuO_6$ (2 K), m(Pr) = 0.46 (4)μ_B and m(Fe/Ru) = 2.24μ_B for $SrPrFeRuO_6$ (2 K), and m(Fe/Ru) = 1.92μ_B for $SrNdFeRuO_6$ (10 K).

1. Introduction

Due to the capacity of perovskite structures ABO_3 to accommodate many elements of the periodic table, materials exhibiting dielectric, piezoferroelectric, optical, superconducting and magnetoresistive properties have been discovered. This type of structure is characterized by a rock-salt arrangement of the *B* cations and have motivated numerous studies where the *B* site is occupied by a mixture of a first-row and a second- or third-row transition metal cation. Examples of these materials are Sr_2FeReO_6 (Kobayashi *et al.*, 1999) and Sr_2FeMoO_6 (Kobayashi *et al.*, 2006), which have been extensively studied due to their high Curie temperatures (400 and 420 K) and their possible applications.

$AA'BB'O_6$ double perovskites: The crystal structures of these materials, depending on the relative size of the *B* and *B'* cations, can show ordered or disordered structures; *B*/Ru cation ordering does not necessarily occur and the cation may also be statistically disordered. In general, larger differences in ionic radii ($\Delta r_{B/B'} = |r_B - r_{B'}|$) are correlated to higher degrees of cation ordering. The crystal structure has been determined either as cubic ($Fm\bar{3}m$), trigonal ($R\bar{3}$), tetragonal ($I4/m$) or monoclinic ($P2_1/n$ or $I2/m$) for ordered structures, and cubic ($Pm\bar{3}m$), trigonal ($R\bar{3}c$) or orthorhombic (*Pbnm*) for disor-

dered ones. Examples of ordered double perovskites are Sr*LnM*RuO$_6$ (*Ln* = La, Pr, Nd; *M* = Co, Ni; Kim & Battle, 1995; Bos & Attfield, 2004; Gateshki & Igartua, 2003; Iturbe-Zabalo, Faik *et al.*, 2013), where the cation difference is $\Delta r_{Ni/Ru} = 0.125$ and $\Delta r_{Co/Ru} = 0.180$ Å; whereas SrLaMnRuO$_6$ ($\Delta r_{Mn/Ru} = 0.06$ Å; Woodward *et al.*, 2008) and SrLaFeRuO$_6$ ($\Delta r_{Fe/Ru} = 0.06$ Å; Shaheen *et al.*, 2008) are disordered.

In a quest to find new prospective materials, three double perovskites differing in the lanthanide cation have been selected, $AA'BB'O_6$ (A = Sr; A' = *Ln* = La, Pr, Nd; B = Fe; B' = Ru). Structural details of SrLaFeRuO$_6$ have been reported in Shaheen *et al.* (2008). In the present work we report a revised crystal and the magnetic structure of this compound. To the best of our knowledge no structural data are available in the literature for the other two perovskites.

In Shaheen *et al.* (2008), on the basis of X-ray powder diffraction (XRPD) patterns, SrLaFeRuO$_6$ was established to be a disordered orthorhombic perovskite, with no ordering of the Fe^{3+} and Ru^{4+} ions in the octahedral sites. Mössbauer spectroscopy in Shaheen *et al.* (2008) shows no magnetic interaction at room temperature.

In the present work we describe the symmetry-mode decomposition and the crystal structure results based on high-resolution neutron powder diffraction (NPD) studies.

2. Experimental

2.1. Sample preparation

Polycrystalline samples of Sr*Ln*FeRuO$_6$ (*Ln* = La, Pr, Nd) were prepared by standard methods of the solid-state reaction. Stoichiometric amounts of $SrCO_3$ (99.995%), La_2O_3 (99.999%) or Pr_2O_3 (99.9%) or Nd_2O_3 (99.9%), RuO_2 (99.9%), Fe_2O_3 (99.98%) were mixed according to the following chemical reaction

$$2SrCO_3 + Ln_2O_3 + 2RuO_2 + Fe_2O_3 \rightarrow 2SrLnFeRuO_6 + 2CO_2 \uparrow \quad (1)$$

All reacting compounds were used as received (all from Sigma-Aldrich). The starting materials were mixed and ground in an agate mortar with acetone and subsequently heated in air, in alumina crucibles. The following heat treatment was used: 24 h at different temperatures, from 770 to 1470 K every 100 K; 48 h at 1520 K. After each heating, the samples were cooled down slowly (3 K min^{-1}) and reground to improve homogeneity. In order to control the quality of the obtained material, X-ray diffraction measurements were performed after each heating. All polycrystalline samples were obtained as dark-grey powders.

In all samples a small amount of impurity was detected: La_3RuO_7 (less than 1%), Pr_3RuO_7 (7.8% weight fraction) and Nd_3RuO_7 (7.6% weight fraction), in SrLaFeRuO$_6$, SrPrFeRuO$_6$ and SrNdFeRuO$_6$, respectively.

2.2. Diffraction measurements

Experimental details are given in Table 1. Room- and high-temperature diffraction data were collected on a Bruker D8 Advance diffractometer equipped with a Våntec high-speed one-dimensional detector (with 3° angular aperture), using Cu $K\alpha$ radiation and an Anton Paar HTK2000 high-temperature chamber with direct sample heating (Pt filament) and a temperature stability of 0.5 K. The specimens for high-temperature measurements were prepared by mixing the material under study with acetone. The mixture was then 'painted' over the Pt-strip heater of the evacuated chamber. In order to obtain reliable values for the unit-cell lattice parameters in the whole temperature range, 48 diffraction patterns were collected between 300 and 1475 K, with a temperature step of 25 K.

Neutron diffraction measurements were performed with the SPODI high-resolution instrument at FRM II (Garching, Germany; Hoelzel *et al.*, 2012), HRPT high-resolution instrument at SINQ-PSI (Villigen, Switzerland; Fischer *et al.*, 2000) and D2B high-resolution and D1B instruments at Institut Laue–Langevin (Grenoble, France). The diffraction profiles at room temperature for SrNdFeRuO$_6$ in the SPODI instrument were collected in the range 2θ = 0–154° with a neutron wavelength of 1.5482 Å. The monochromator was Ge(551). This instrument is equipped with a detector that covers 160° in 2θ space and is made of 80 ^{3}He tubes. The measurements were carried out using a vanadium can of 8 mm in diameter. The diffraction profiles for SrPrFeRuO$_6$ in the HRPT instrument were collected in the range 2θ = 0–160° with a neutron wavelength of 1.494 Å, between 300 and 1400 K. This instrument is equipped with a linear position-sensitive ^{3}He detector with 1600 wires and angular separation of 0.1°, that covers 160° in 2θ space. Room- and high-temperature measurements were performed using a vanadium can of 8 mm in diameter. The collection of the profiles in a D2B instrument for SrLaFeRuO$_6$ was carried out in the range 2θ = 0–160° with a neutron wavelength of 1.594 Å, between room temperature and 1173 K. The monochromator was Ge (335) with $\Delta d/d \simeq 5 \times 10^{-4}$ resolution. This instrument is equipped with a detector that covers 160° in 2θ space and is made of 128 ^{3}He tubes. The samples were placed in a vanadium can of 8 mm in diameter. Profiles obtained in D1B for all the compounds were collected in the range 2θ = 0–128°, between 2 and 300 K. This instrument was operated with a wavelength of 2.52 Å produced by a high-mosaicity pyrolytic graphite monochromator; even though a set of filters were installed between monochromator and sample in order to avoid the high-order contaminations, a non-negligible amount of $\lambda/2$ contamination was observed in some cases (*ca* 0.3%). D1B is equipped with a ^{3}He multi-detector containing 1280 cells. The samples were placed in a vanadium can of 5 mm in diameter. The coherent scattering lengths for the elements are: 7.02 fm (Sr), 8.24 fm (La), 4.58 fm (Pr), 7.69 fm (Nd), 9.45 fm (Fe), 7.03 fm (Ru) and 5.805 fm (O).

Synchrotron radiation diffraction measurements were performed at the BM25-Branch A high-resolution powder diffractometer at Spline-ESRF (Grenoble, France). The diffraction profiles were collected in the range 2θ = 9–50° with a wavelength of 0.8256 Å at 300 K.

Table 1
Experimental details.

Sample	$SrLaFeRuO_6$ $SrPrFeRuO_6$ $SrNdFeRuO_6$	$SrPrFeRuO_6$	$SrLaFeRuO_6$ $SrPrFeRuO_6$ $SrNdFeRuO_6$	$SrLaFeRuO_6$ $SrPrFeRuO_6$	$SrNdFeRuO_6$	$SrPrFeRuO_6$	$SrLaFeRuO_6$ $SrPrFeRuO_6$ $SrNdFeRuO_6$
Temperature (K)	300	300–1475	300	300	300	400–1400	2–600
Radiation type	X-ray	X-ray	Synchrotron	Neutron	Neutron	Neutron	Neutron
Diffractometer	Bruker D8 Advance	Bruker D8 Advance	BM25-brach A (ESRF)	D2B (ILL)	SPODI (FRMII)	HRPT (SINQ)	D1B (ILL)
Wavelength (Å)	Cu $K\alpha_1$	Cu $K\alpha_1$ and $K\alpha_2$	0.8256	1.594	1.5482	1.494	2.52
Purpose exp.	Symmetry/lattice amplimodes	Phase transition amplimodes	Symmetry/lattice amplimodes	Mode refinement	Mode refinement	HT mode refinement	Magnetic structure
Information	–	–	–	Tables 3 and 5	Tables 3 and 5	Table 6	Tables 7 and 8

Computer programs: *AMPLIMODES* (Orobengoa *et al.*, 2009), *FullProf* suite (Rodríguez-Carvajal, 1993) and *SARAh* (Wills, 2000).

2.3. Analysis of the diffraction data

Rietveld refinement (Rietveld, 1969) of the structures was performed using AMPLIMODES for *FullProf* (Orobengoa *et al.*, 2009), located in the Bilbao Crystallographic Server (Aroyo, Perez-Mato *et al.*, 2006; Aroyo, Kirov *et al.*, 2006), and *WinPlotr*/*FullProf* package (Rodríguez-Carvajal, 1993). The peak shape was described by a pseudo-Voigt function, and the background level was modeled using a polynomial function. The refined parameters were: scale factor, zero-shift, lattice parameters, peak profile (two asymmetry parameters), atomic positions [atomic positions (amplitudes of the modes transforming according to the irreps (collective displacements)) instead of the atomic coordinates] and independent isotropic atomic displacement parameters. In the case of the synchrotron radiation data, the resolution function provided at the instrument was used.

The symmetry-adapted mode analysis was used for the powder-diffraction pattern analysis. The structures proposed in Iturbe-Zabalo, Faik *et al.* (2013) for ordered $SrNdMRuO_6$ and $SrPrMRuO_6$ perovskites were the starting point for analysis of the disordered double perovskites presented in this work. The difference between the ordered and disordered double perovskites is the high-symmetry archetype phase: $Fm\bar{3}m$ for the ordered case and $Pm\bar{3}m$ when disorder is present.

The initial structural information needed for the symmetry-adapted mode analysis (Iturbe-Zabalo, Faik *et al.*, 2013; Iturbe-Zabalo, Igartua *et al.*, 2013; Orobengoa *et al.*, 2009; Faik *et al.*, 2009) is: the reference structure (the archetype cubic phase, space group $Pm\bar{3}m$; atomic positions and lattice parameters); the lattice parameters and space group of the room-temperature phase; and finally, the transformation matrix between both cells (Table 2). We have reported a complete description of the procedure in Iturbe-Zabalo, Faik *et al.* (2013).

Representation analysis of the possible magnetic moment arrangements was carried out using the *SARAh* representation analysis program (Wills, 2000) and *BasIreps* program, included in the *FullProf* Suite package. Analysis of the magnetic structures was carried out using *FullProf*.

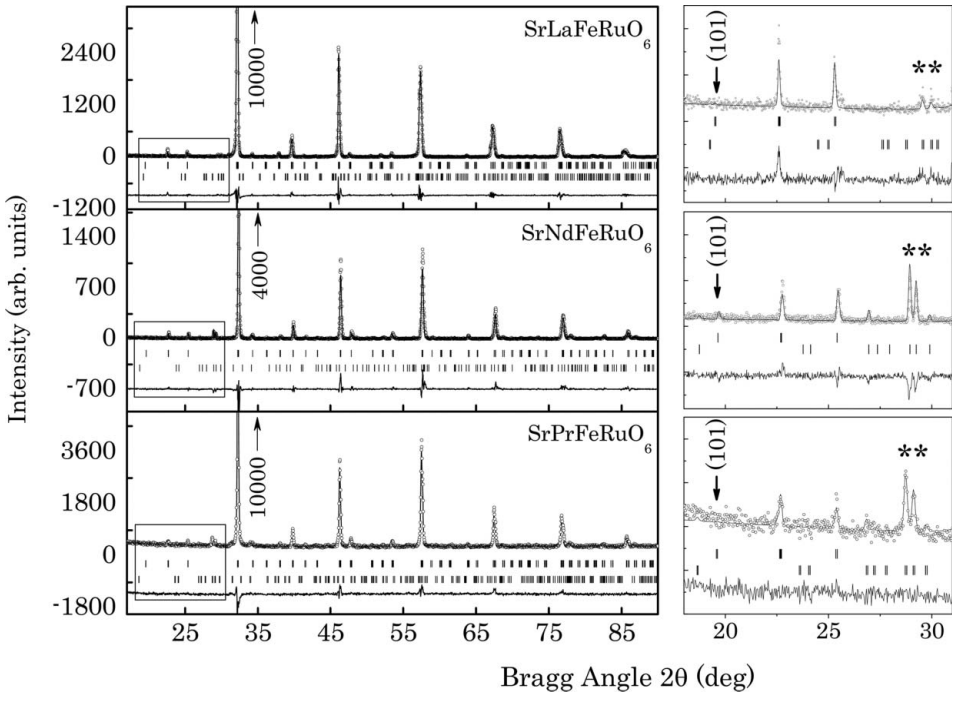

Figure 1
Experimental (symbols) and calculated (line) X-ray powder diffraction profiles for the Rietveld refinement of $SrLnFeRuO_6$ (*Ln* = La, Nd, Pr) at room temperature, using a disordered orthorhombic (*Pbnm*) structural model. The upper (lower) markers indicate the position of the structural $SrLnFeRuO_6$ [impurity: La_3RuO_7 (space group *Cmcm*), Nd_3RuO_7 (space group *Cmcm*) and Pr_3RuO_7 (space group *Cmcm*)] Bragg reflections. The inset shows the absence of the superstructure reflection, indicated with an arrow; * indicates the impurity.

3. Results and discussion

3.1. Room-temperature structures

Room-temperature XRPD data for $SrLaFeRuO_6$, $SrPrFeRuO_6$ and

$SrNdFeRuO_6$ are shown in Fig. 1. In the insets of Fig. 1 the positions of the B/B' ordering superstructure reflections are marked around $2\theta = 19.5^\circ$ with arrows, making clear the absence of such reflections. This fact indicates that these compounds do not present an ordered arrangement of the *B*-site cations, and therefore only space groups allowing disorder were considered (Woodward, 1997). In fact, the orthorhombic *Pbnm* space group has been proposed for the room-temperature structure of $SrLaFeRuO_6$ (Shaheen *et al.*, 2008); hence, we used this space group as the starting model for our refinements. After the XRPD data refinement, the space group *Pbnm* (*International Tables for Crystallography*, Vol. A, ITA, No. 62 non-standard setting of *Pnma*) should be assigned to $SrLaFeRuO_6$, $SrPrFeRuO_6$ and $SrNdFeRuO_6$ compounds.

The structures of the title compounds were refined from neutron powder diffraction (NPD) data in the *Pbnm* space group (Fig. 2), with the unit-cell lattice parameters chosen as $a \sim b \simeq (2)^{1/2}a_p$, $c \simeq 2a_p$ (a_p is the cubic archetype simple perovskite lattice parameter) and with the following atomic positions: Sr/*Ln* 4*c* (x,y,1/4), Fe/Ru 4*a* (0,$\frac{1}{2}$,0), O1 4*c* (x,y,1/4) and O2 8*d* (x,y,z).

The intensity of some of the reflections was not possible to properly fit the orthorhombic structural model and a magnetic model was necessary to be included at room temperature (see §3.3). Detailed information of the refinements is given in Table 3.

Table 4 lists selected interatomic distances and bond angles. The average ⟨Fe/Ru—O⟩ bond lengths in the octahedra are 1.991 (2), 1.994 (2) and 1.993 (2) Å for $SrLaFeRuO_6$, $SrPrFeRuO_6$ and $SrNdFeRuO_6$, respectively. These values are close to 2.03 Å, the distance calculated from the effective ionic radii (Shannon, 1976) for Fe/Ru—O. The Sr^{2+}/Ln^{3+} cations are located in the cavities formed by the corner-sharing Fe/RuO_6 octahedra. The average ⟨Sr/*Ln*—O⟩ distances, shown in Table 4, are typical for Sr^{2+}/Ln^{3+} disordered cations in a ninefold coordination. The bond-valence method (Brown & Altermatt, 1985) allowed us to have an estimation of the oxidation states of the Fe and Ru cations. The calculated valences, shown in Table 4, suggest that Fe is trivalent and Ru is present in a tetravalent oxidation state. Regarding the Sr/*Ln*—O distances, there is no notable difference among the three compounds; with a slightly larger distance for Sr/La—O caused by the larger size of the La cation. Being larger induces a smaller tilt in the octahedra, which in turn increases the distance. The higher variation for the Fe/Ru—O bond-length values reported in Shaheen *et al.* (2008) for $SrLaFeRuO_6$ could be due to the experimental method (XRPD) used in Shaheen *et al.* (2008): the scattering power of O atoms compared with the rest of the cations of the structure is low for X-rays and, hence, the lower the

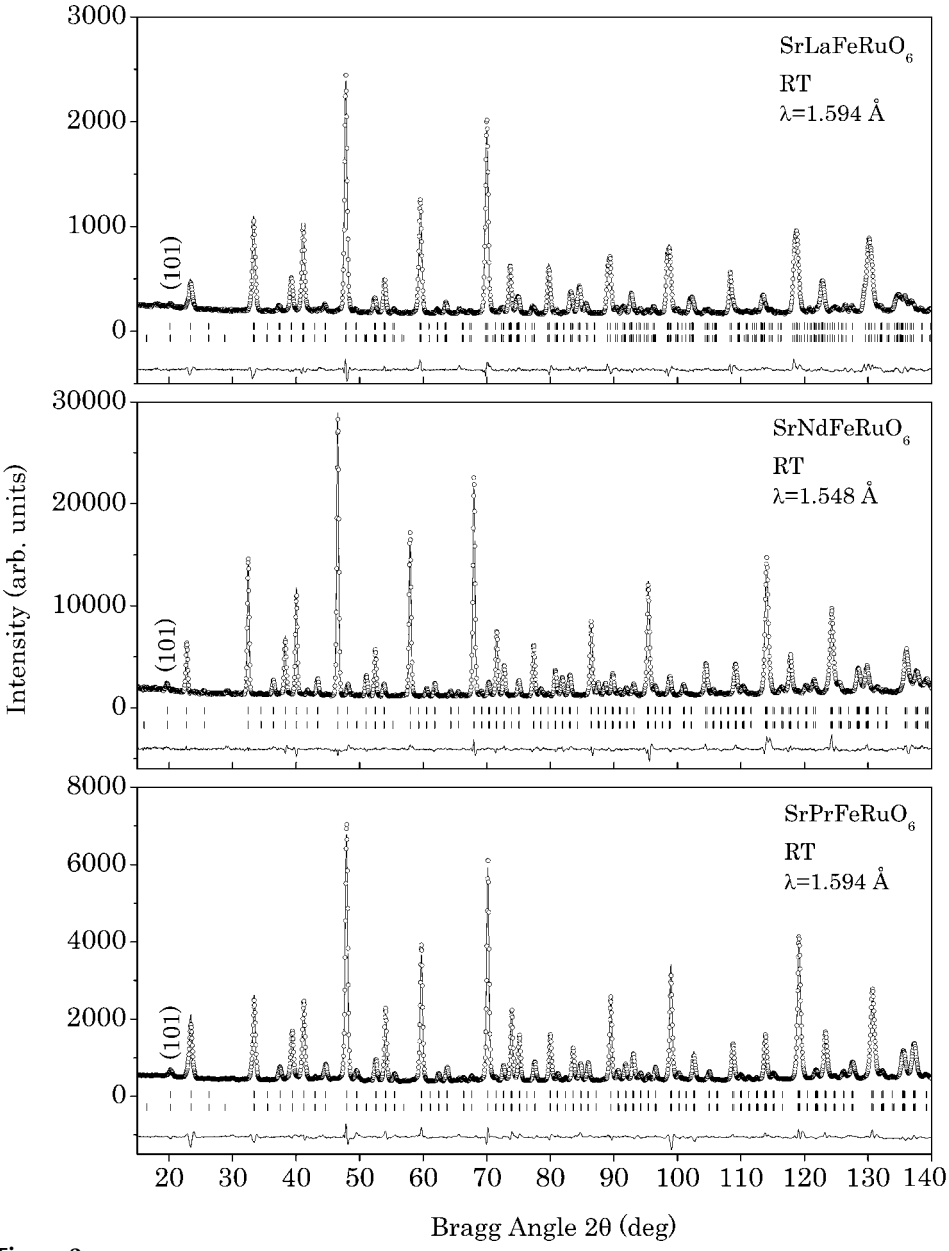

Figure 2
Experimental (symbols) and calculated (line) neutron powder diffraction profiles for the Rietveld refinement of Sr*Ln*$FeRuO_6$ (*Ln* = La, Nd, Pr) at room temperature, using a disordered orthorhombic (*Pbnm*) structural model. The upper (middle) markers indicate the position of the structural (magnetic) Bragg reflections and the lower markers the impurity (Nd_3RuO_7 and Pr_3RuO_7) Bragg reflections. The La_3RuO_7 impurity was excluded in order to guarantee convergence of the refinement.

Table 2
Input information for *AMPLIMODES* for *FullProf*: high-symmetry phase information (virtual prototype structure), low-symmetry structure information (lattice parameters obtained by XRPD data refinement) and transformation matrix.

$Pm\bar{3}m$ (ITA No. 221, standard setting), *Pbnm* (ITA No. 62, non-standard setting) and $R\bar{3}c$ (ITA No. 167, standard setting).

High-symmetry structure					
221					
3.8438	3.8438	3.8438	90.00	90.00	90.00
4					
Fe	1	1*a*	0.00000	0.00000	0.00000
Sr	1	1*b*	0.50000	0.50000	0.50000
O	1	3*d*	0.00000	0.00000	0.50000
Low-symmetry structure					
062					
5.5350	5.5434	7.8246	90.00	90.00	90.00
Transformation matrix	$\left(\begin{array}{ccc\|c} 1 & 1 & 0 & 1/2 \\ -1 & 1 & 0 & 1/2 \\ 0 & 0 & 2 & 0 \end{array}\right)$				
Low-symmetry structure					
167					
5.5973	5.5973	13.7181	90.00	90.00	120.00
Transformation matrix	$\left(\begin{array}{ccc\|c} 0 & 1 & 2 & 0 \\ -1 & 0 & 2 & 0 \\ 1 & -1 & 2 & 0 \end{array}\right)$				

Table 3
Structural details of SrLaFeRuO6, $SrPrFeRuO_6$ and $SrNdFeRuO_6$ obtained at room temperature from NPD data using the *Pbnm* structural model, refining all mode amplitudes.

The B_{iso} value for Fe/Ru cations was fixed in 0.5 Å in order to guarantee the convergence of the refinement.

		$SrLaFeRuO_6$	$SrPrFeRuO_6$	$SrNdFeRuO_6$
Instrument		D2B (ILL)	D2B (ILL)	SPODI (FRMII)
Sr/*Ln*	4*c* (*x*, *y*, 1/4)			
	x	0.0000 (9)	0.001 (1)	0.0023 (7)
	y	−0.0166 (6)	−0.0245 (5)	−0.0294 (3)
	B_{iso} (Å^2)	0.66 (3)	0.56 (3)	0.24 (2)
Fe/Ru	4*a* (0, $\frac{1}{2}$, 0)			
	B_{iso} (Å^2)	0.5	0.5	0.5
O1	4*c* (*x*, *y*, 1/4)			
	x	−0.0661 (7)	−0.0790 (5)	−0.0837 (5)
	y	0.507 (1)	0.5096 (7)	0.5089 (6)
	B_{iso} (Å^2)	0.89 (2)	0.81 (2)	0.67 (2)
O2	8*d* (*x*, *y*, *z*)			
	x	0.7277 (5)	0.7223 (5)	0.7229 (4)
	y	0.2719 (5)	0.2784 (5)	0.2790 (4)
	z	0.5289 (3)	0.5291 (3)	0.5298 (3)
	B_{iso} (Å^2)	0.89 (2)	0.81 (2)	0.67 (2)
a (Å)		5.5752 (2)	5.5477 (2)	5.5357 (2)
b (Å)		5.5463 (2)	5.5463 (2)	5.5432 (2)
c (Å)		7.8557 (3)	7.8390 (2)	7.8257 (3)
V (Å^3)		242.91 (2)	241.20 (2)	240.13 (1)
R_p		0.038	0.038	0.047
R_{wp}		0.048	0.049	0.063
R_{exp}		0.061	0.038	0.023
R_{Bragg}		0.055	0.047	0.075

Table 4
Bond lengths (Å), octahedra tilt angles (°), selected angles (°) and bond-valence sums for $SrLnFeRuO_6$ (*Ln* = La, Pr, Nd) at room temperature obtained from NPD data using the *Pbnm* structural model and refining all mode amplitudes.

Sr/*Ln*—O distance in nine coordination is chosen since it is the highest coordination number available for all tabulated rare-earths.

	$SrLaFeRuO_6$	$SrPrFeRuO_6$	$SrNdFeRuO_6$
Sr/*Ln*—O1 (×1)	2.668 (7)	2.621 (5)	2.603 (4)
Sr/*Ln*—O1 (×1)	2.927 (7)	2.995 (5)	3.022 (4)
Sr/*Ln*—O1 (×1)	2.423 (6)	2.347 (7)	2.327 (5)
Sr/*Ln*—O1 (×1)	3.159 (6)	3.213 (7)	3.225 (5)
Sr/*Ln*—O2 (×2)	3.109 (4)	3.161 (4)	3.180 (3)
Sr/*Ln*—O2 (×2)	2.544 (4)	2.525 (4)	2.527 (3)
Sr/*Ln*—O2 (×2)	2.791 (4)	2.741 (4)	2.734 (3)
Sr/*Ln*—O2 (×2)	2.707 (4)	2.710 (5)	2.683 (3)
$\langle$Sr/*Ln*—O2 (×2)$\rangle_{coord.9}$	2.68 (1)	2.66 (1)	2.65 (1)
Tilt angle $\Psi_{[001]P}$	5.05 (7)	6.37 (6)	6.39 (5)
Tilt angle $\Phi_{[110]P}$	10.70 (1)	12.71 (1)	13.48 (1)
Fe/Ru—$O1_{ax}$ (×2)	1.999 (1)	2.009 (1)	2.011 (1)
Fe/Ru—$O2_{eq}$ (×2)	1.984 (3)	1.989 (3)	1.992 (2)
Fe/Ru—$O2'_{eq}$ (×2)	1.989 (3)	1.984 (3)	1.977 (2)
Average distance	1.99 (1)	1.99 (1)	1.99 (1)
$\angle O1_{ax}$—Fe/Ru—$O2_{eq}$	89.1 (1)	87.7 (1)	87.2 (1)
$\angle O1_{ax}$—Fe/Ru—$O2'_{eq}$	91.2 (1)	92.5 (1)	92.7 (1)
$\angle O2_{eq}$-Fe/Ru-$O2'_{eq}$	91.0 (1)	90.8 (1)	90.8 (1)
∠Fe/Ru—$O1_{ax}$—Ru/Fe	158.6 (2)	154.6 (2)	153.2 (2)
∠Fe/Ru—$O2_{eq}$—Ru/Fe	163.5 (2)	161.6 (2)	161.4 (2)
Bond-valence sum			
Fe	3.21 (1)	3.18 (1)	3.19 (1)
Ru	3.93 (1)	3.90 (1)	3.90 (1)

reliability of the oxygen positions compared with those from NPD.

The mode decomposition suggests that there are five irreducible representations (irreps) of the $Pm\bar{3}m$ space group that take part in symmetry breaking from that space group to the room-temperature *Pbnm* orthorhombic space group: $R_4^+(1)$, $R_5^+(2)$, $X_5^+(2)$, $M_2^+(1)$ and $M_3^+(1)$; theoretical considerations show (Howard & Stokes, 1998, 2005; Perez-Mato *et al.*, 2010) that there is no single irrep that breaks the symmetry from $Pm\bar{3}m$ to *Pbnm* (Fig. 3). At least two modes are needed: R_4^+ and M_3^+.

Looking at the amplitudes of the modes transforming according to the irreps in Table 5, it is clear that there are two global amplitudes (R_4^+ and M_3^+) that are higher than the rest. X_5^+ is less than half the value of M_3^+, and R_5^+ and M_2^+ have negligible values. Despite the fact that some of the amplitudes of these modes could be excluded from the refinement process, it has to be taken into account that the experimental data should be respected, and all the structural information in Tables 3 and 4 has been obtained refining all the amplitudes. However, for some studies, like phase-transition studies, the refinement can be simplified by using only some of the allowed degrees of freedom. To illustrate the effect of the reduction of degrees of freedom, three refinement attempts have been done, Table 5:

(i) freed all mode amplitudes,

Table 5
NPD data refinement results for the amplitudes (in Å) of irreps taking part in symmetry breaking from the space group $Pm\bar{3}m$ to the room-temperature *Pbnm* orthorhombic space group, refining (*a*) all the modes and (*b*) 3 and (*c*) 2 highest amplitudes modes for Sr*Ln*FeRuO$_6$ (*Ln* = La, Pr, Nd) compounds.

			Amplitude								
			LaFe			PrFe			NdFe		
Irrep	Isotropy subgroup	Dim	(*a*)	(*b*)	(*c*)	(*a*)	(*b*)	(*c*)	(*a*)	(*b*)	(*c*)
R_4^+	*Imma* (74)	1	0.980 (4)	0.974 (4)	0.971 (4)	1.085 (4)	1.047 (3)	1.045 (4)	1.133 (4)	1.086 (4)	1.089 (6)
R_5^+	*Imma* (74)	2	0.07 (1)	0.00	0.00	0.165 (7)	0.00	0.00	0.193 (7)	0.00	0.00
X_5^+	*Cmcm* (63)	2	0.201 (8)	0.195 (8)	0.00	0.294 (6)	0.266 (6)	0.00	0.344 (4)	0.327 (4)	0.00
M_2^+	*P*4/*mbm* (127)	1	0.01 (1)	0.00	0.00	0.01 (1)	0.00	0.00	0.021 (9)	0.00	0.00
M_3^+	*P*4/*mbm* (127)	1	0.494 (7)	0.500 (7)	0.522 (7)	0.627 (4)	0.674 (4)	0.695 (5)	0.627 (5)	0.686 (5)	0.736 (7)
R_p			0.038	0.038	0.041	0.038	0.040	0.045	0.047	0.052	0.067
R_{wp}			0.048	0.048	0.053	0.049	0.051	0.060	0.063	0.068	0.095
R_{exp}			0.061	0.061	0.061	0.038	0.038	0.038	0.023	0.023	0.023
R_{Bragg}			0.055	0.058	0.065	0.047	0.058	0.069	0.075	0.090	0.120

K-vector: R_4^+ $(\frac{1}{2},\frac{1}{2},\frac{1}{2})$, R_5^+ $(\frac{1}{2},\frac{1}{2},\frac{1}{2})$, X_5^+ $(0,\frac{1}{2},0)$, M_2^+ $(\frac{1}{2},\frac{1}{2},0)$, M_3^+ $(\frac{1}{2},\frac{1}{2},0)$
Direction: R_4^+ $(0,a,a)$, R_5^+ $(0,a,-a)$, X_5^+ $(0,0,0,-a,0,0)$, M_2^+ $(a,0,0)$, M_3^+ $(a,0,0)$

(ii) set to zero the amplitudes of the modes transforming according to R_5^+ and M_2^+, and finally,

(iii) freed only R_4^+ and M_3^+ modes.

The effect of the three approaches on the reliability factors of the refinements is clear: the more symmetric the structure at room temperature the smaller the effect when R_5^+ and M_2^+ are set to zero (Tables 5*a* and *b*). This is clearly observed for SrLaFeRuO$_6$: all modes with amplitudes close to zero could be nullified, with an increment in the *R* factors of less than 3%. For the other two compounds, which are less symmetric at room temperature, the effect of reduction of the refined mode amplitudes on the reliability factors is larger (increment of the *R* factors around 20%). Nevertheless, although the reduction in degrees of freedom increases the inaccuracy of atomic positions, the refinements done in this way could be enough to study the structural phase transitions. The third refinement attempt (iii) suggests that although the X_5^+ mode is not one of the active modes, it is necessary to describe the structure and should be kept in the refinement.

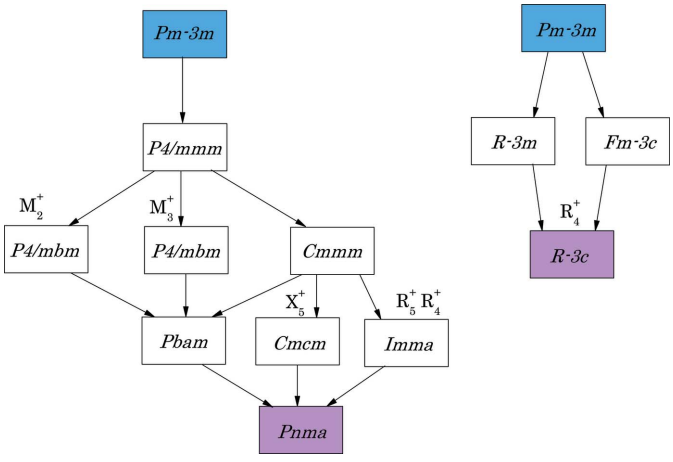

Figure 3
Graph of maximal subgroups relating the space group of the archetype (highlighted in blue) and distorted *Pbnm* and *R*3 phase (highlighted in pink) of Sr*Ln*FeRuO$_6$. For each subgroup any irrep yielding this symmetry is indicated.

The geometrical representations of the distortion modes, taking as a reference the orthorhombic cell, are shown in Fig. 4. The physical interpretation of the modes taking part in symmetry breaking is the tilting of the octahedra. If the values of the mode amplitudes are small and are defined in one-dimensional space, these are linearly related to the tilts of the octahedra: $a^+b^-b^-$ tilt system (*Pbnm*; Glazer, 1972, 1975). The variation of the obtained mode amplitudes (and octahedral tilt angles) *versus* the tolerance factors is plotted in Fig. 5. It shows

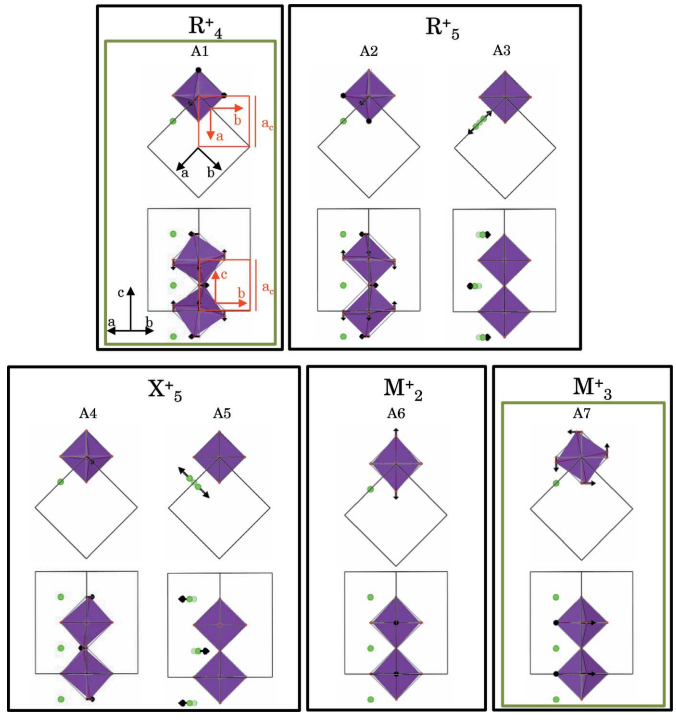

Figure 4
Schematic representation of the five irrep distortions allowed in the *Pbnm* configuration, corresponding to M_2^+, M_3^+, R_4^+, R_5^+ and X_5^+. Fe/Ru disordered octahedra in purple, the *A*/*A*′-site Sr/*Ln* cations in green and O atoms in red. As a reference, the simple perovskite cubic cell (red) and the double perovskite orthorhombic cell (black) are also plotted. The polarization vectors are shown by small black arrows.

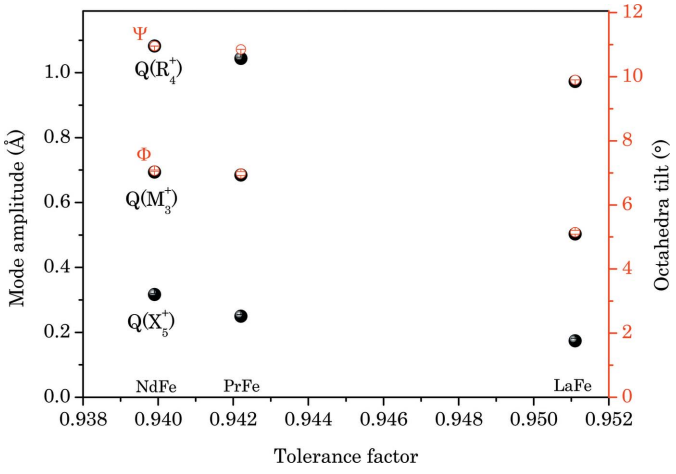

Figure 5
Amplitudes of R_4^+, M_3^+ and X_5^+ irreps conforming the room-temperature phase of the SrLaFeRuO$_6$, SrPrFeRuO$_6$ and SrNdFeRuO$_6$ compounds, and Ψ and Φ tilt angles, as obtained from the NPD data refinement (3 mode refined), as a function of the tolerance factors. The tolerance factors are calculated with the Sr/*Ln*—O distance in nine coordination. Ψ and Φ represent the rotation of octahedra about the pseudo-cubic $[110]_p$ and $[001]_p$ axes, respectively.

a clear trend: the less distorted the structure, the smaller the amplitudes of the modes. Among the SrLaFeRuO$_6$, SrPrFeRuO$_6$ and SrNdFeRuO$_6$ compounds, the former is less distorted. This observation is in perfect agreement with the fact that the La cation is larger than Pr and Nd, needing a bigger cubo-octahedral space and preventing the tilt of the octahedra. Hence, the smaller the value of the mode amplitudes, the smaller the tilting of the octahedra and the more symmetric the structure at room temperature. SrLaFeRuO$_6$, with the smallest symmetry-mode amplitude values, is the more symmetric of the three reported here.

3.2. High-temperature structural phase transitions: SrPrFeRuO$_6$

The thermal evolution of SrPrFeRuO$_6$ was studied by means of laboratory X-ray powder diffraction measurements at different temperatures. As mentioned in §1, several different symmetries have been reported for disordered double perovskites at room temperature, however, only a few temperature-dependent structural studies have been done. To search for structural phase transitions in our sample we analyzed the intervals 24–26° and 93–96° corresponding to the (111) primitive cell peak and (321) cubic cell reflections, shown in Fig. 6. In the first 2θ range diminishing intensity was clearly observed on heating and, at about 1075 K, the reflections of the type *hkl*, with $h + k + l = 2n + 1$, disappear, indicating a structural phase transition from a primitive to a non-primitive space group. One of the usual intermediate space groups is the trigonal $R\bar{3}c$ (Horikubi *et al.*, 1999). XRPD and NPD data at 1200 K confirm $R\bar{3}c$ to be the space group of the intermediate phase. The structural information for SrPrFeRuO$_6$ at 1200 K is presented in Table 6 and the evolution of the lattice parameters with temperature is shown in Fig. 7. It is not the first time that the *Pbnm* → $R\bar{3}c$ structural phase transition is observed in double perovskites (Horikubi *et al.*, 1999).

In the symmetry breaking from cubic archetype ($Pm\bar{3}m$) to the trigonal ($R\bar{3}c$) phase, there is a single irrep that takes part: R_4^+. That mode displaces the O atoms of the asymmetric unit along the *a* axis.

There is no group/subgroup relation between the orthorhombic *Pbnm* and trigonal $R\bar{3}c$ space

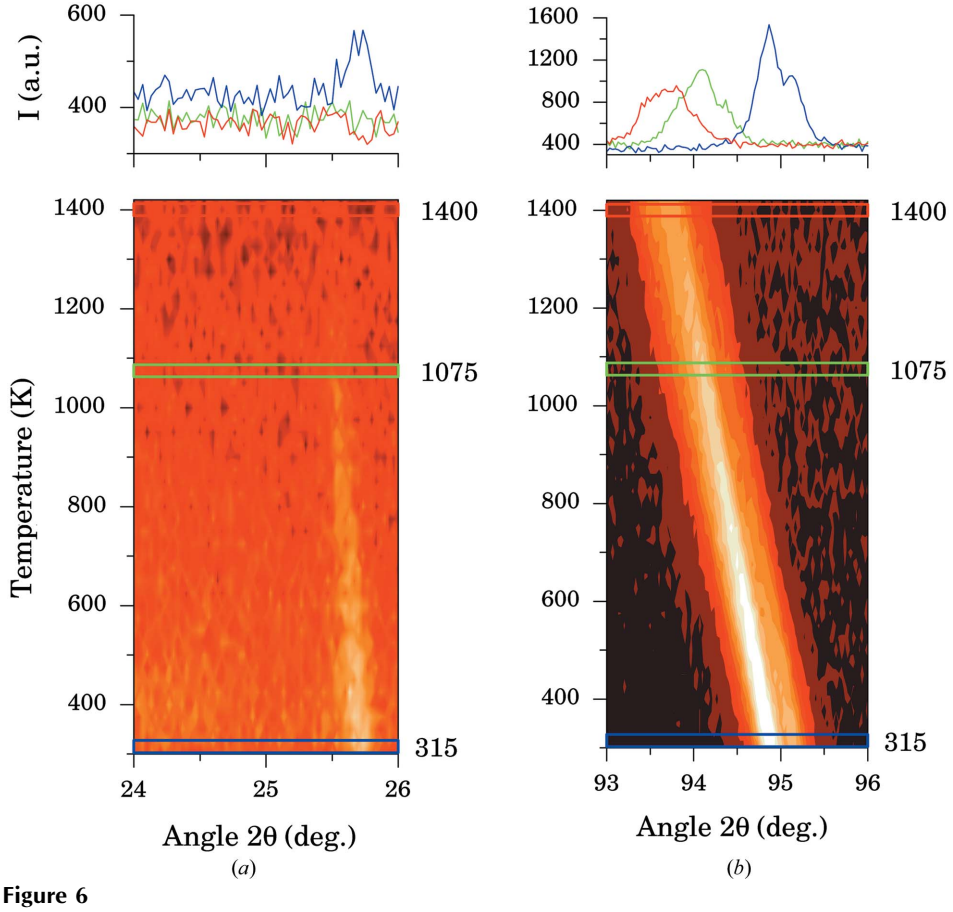

Figure 6
Thermal evolution of the (111) primitive peak and (321) cubic reflections of SrPrFeRuO$_6$ obtained from the XRPD experiment. The scattered intensity is represented with yellow–red scale, light-yellow being high intensity and dark-red the lowest intensity. At 1075 K the intensity of the peaks related to the primitive cell disappear, transforming into a trigonal cell.

Table 6
Crystal structure data and refinement results for $SrPrFeRuO_6$ from NPD (HRPT, PSI) at 1200 K using the $R\bar{3}c$ model.

Reliability factors	Lattice parameters	Atom	Site	x	y	z	B_{iso} (Å^2)	Occupancy
R_p = 0.041	a = 5.5977 (2) Å	Sr/Pr	6a	0.0000	0.0000	0.2500	2.52 (4)	0.5/0.5
R_{wp} = 0.0553	c = 13.720 (1) Å	Fe/Ru	6c	0.0000	0.0000	0.0000	1.02 (2)	0.5/0.5
R_{exp} = 0.0334	γ = 120°	O1	18e	0.5424 (3)	0.0000	0.2500	3.42 (3)	1
R_{Bragg} = 0.101	V = 372.31 (3) Å^3							

Irrep	K vector	Dir.	Iso. subgroup	Dim	Amplitudes (Å)
R_4^+	$(\frac{1}{2},\frac{1}{2},\frac{1}{2})$	(a, a, a)	$R\bar{3}c$	1	0.571 (5)

groups (Fig. 3). This means that the structural phase transition experimentally observed between the room-temperature structure and the intermediate phase will be first order (discontinuous). Both phases can be referred to the same cubic archetype phase. As it is very common in many distorted double perovskite compounds (Gateshki & Igartua, 2003) and, in particular, in this sample, owing to experimental limitations, no cubic phase is known. Thus, a virtual archetype cubic phase is used as the reference structure (Table 2).

Despite the fact that the irreps lowering successively the symmetry from cubic to trigonal ($R\bar{3}c$) and from cubic to orthorhombic (*Pbnm*) involve mainly oxygen displacements, the cubic-to-trigonal phase transition is continuous (second order); while, as mentioned, the trigonal-to-orthorhombic transition is discontinuous (first order).

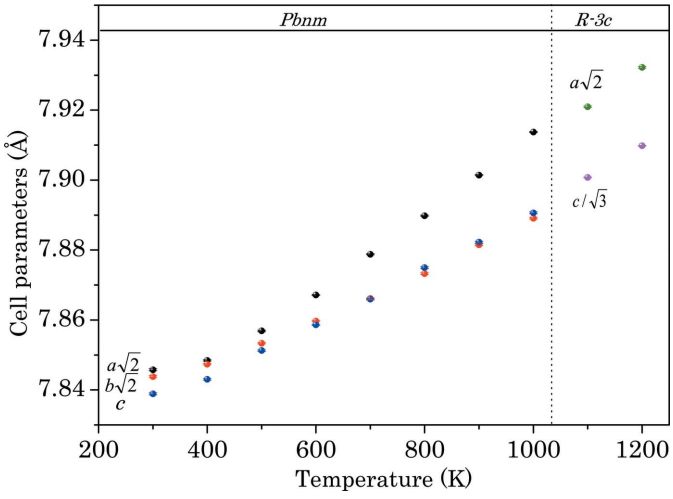

Figure 7
Temperature evolution of the lattice parameters of $SrPrFeRuO_6$ as obtained from the NPD measurements: lattice parameters of the orthorhombic and trigonal phase. The parameters have been scaled to the setting of the double perovskite cubic structure, $a_c = 2a_p$, for comparison.

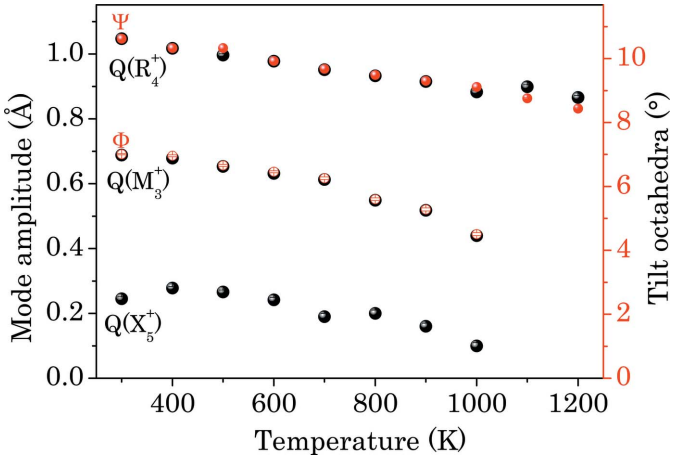

Figure 8
Temperature dependence of the amplitudes of the irreps conforming the *Pbnm* and $R\bar{3}c$ structure of $SrPrFeRuO_6$, and Ψ and Φ tilt angles, as obtained from the NPD data refinement. The amplitudes of the irreps in the high-symmetry phase have been scaled (multiplied by 3/2) to see the evolution, since the program *AMPLIMODES* uses the normalization mode within the corresponding primitive unit cell.

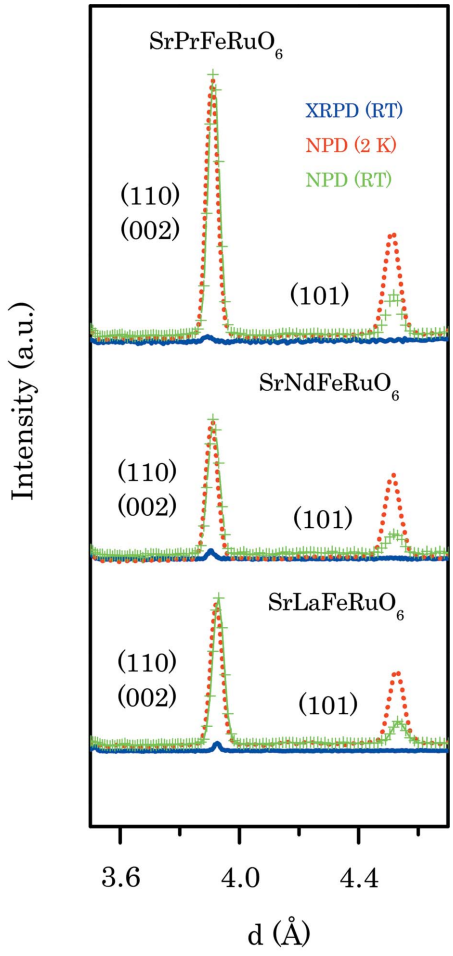

Figure 9
XRPD data at room temperature (blue line), NPD data at 2 K (red dotted line) and room temperature (green crossed line) in d space (in Å). All patterns are re-normalized with respect to the peak height of the main (112/200) index peak at $2\theta \simeq 32.6°$ ($d \simeq 2.7$ Å).

Table 7
Magnetic moment components (in μ_B) determined for each Pr and Fe/Ru site and Rietveld reliability factors for Sr*Ln*FeRuO$_6$ (*Ln* = La, Nd, Pr).

		SrLaFeRuO$_6$ (2 K)	SrPrFeRuO$_6$ (2 K)	SrNdFeRuO$_6$ (10 K)
Γ_{mag}		$3\Gamma_5$	$3\Gamma_3 \oplus 1\Gamma_3$	$3\Gamma_3$
Pr(4*c*)	m_z	–	0.63 (9)	–
	m_{TOT}	–	0.63 (9)	–
Fe/Ru(4*a*)	m_x	0.74 (7)	1.89 (1)	1.81 (1)
	m_y	0.43 (4)	0.28 (4)	0.12 (8)
	m_z	1.67 (1)	−0.16 (9)	1.07 (5)
	m_{TOT}	1.88 (3)	1.92 (3)	2.01 (3)
R_p		0.015	0.016	0.014
R_{wp}		0.022	0.023	0.019
R_{exp}		0.008	0.008	0.009
R_{Bragg}		0.033	0.066	0.046
R_{mag}		0.046	0.070	0.045

Although the structural phase transitions in these kinds of materials essentially originated from the tilting of the octahedra, some of them are continuous while others are discontinuous. In fact, a continuous reduction of the octahedral tilts in the trigonal phase gives rise to a continuous phase transition between trigonal and cubic. The discontinuous character of the orthorhombic-to-trigonal phase transition is related to the change in direction of the R_4^+ (same) irrep, in three-dimensional representation space, as can be seen in Tables 5 and 6. The direction of R_4^+ for the *Pbnm* phase is $(0, a, -a)$, while it changes to (a, a, a) for the trigonal phase.

To study the thermal evolution of the amplitudes of the symmetry-adapted modes we have measured SrPrFeRuO$_6$ by means of NPD. From Table 4 can be concluded that even excluding some mode-amplitudes from the refinements, the obtained biased results 'are not far away' from the real ones, and the exclusion of some modes could be done in a first approximation. In Fig. 8 we show the temperature evolution of the amplitudes of R_4^+, M_3^+ and X_5^+ modes (the rest are negligible) in the orthorhombic phase and the single active mode R_4^+ in the trigonal phase. Although the highest amplitude in the orthorhombic phase and the amplitude in the trigonal, R_4^+, have the same label, the irrep taking part in symmetry breaking from the cubic to the orthorhombic and from the cubic to the trigonal are not the same: the acting direction of each irrep is different. Together with the mode amplitudes, we show the octahedral tilts in Fig. 8. The correlation between the mode amplitudes and tilt angles is very good.

3.3. Magnetic structures

Based on the observation of the NPD patterns at room temperature, neutron diffraction experiments were undertaken at low temperature to determine the magnetic structures. The compounds were analyzed from a set of NPD patterns collected at the D1B instrument in ILL (Grenoble) with λ = 2.52 Å (see §2.1). The La- and Pr-containing compounds were measured at 2 K; whereas SrNdFeRuO$_6$ was measured at 10 K, due to experimental limitations.

The neutron powder diffraction patterns of SrLaFeRuO$_6$, SrPrFeRuO$_6$ and SrNdFeRuO$_6$ show an increase in intensity in some low-angle reflections, which the nuclear model is not able to refine correctly and are not visible in XRPD patterns (see Fig. 9). These peaks have been related to magnetic ordering and from Fig. 10 the magnetic ordering temperatures are *ca* 450, *ca* 475 and *ca* 430 K for Sr*Ln*FeRuO$_6$ (*Ln* = La, Pr, Nd), respectively.

None of the compounds undergo a structural phase transition between room temperature and the lowest temperature measured. However, the change in intensity of some nuclear reflections is observed, in particular at low angles, and no new reflections appear decreasing the temperature; this fact suggests **k** = (0,0,0) to be the propagation vector for the three compounds. As the magnetic scattering factor for Ru^{4+} is not available, the magnetic structures were refined using the scattering factor of Ru^{+}, an approximation used by Hong *et al.* (2000).

To determine the possible magnetic structures compatible with the symmetry of the crystal

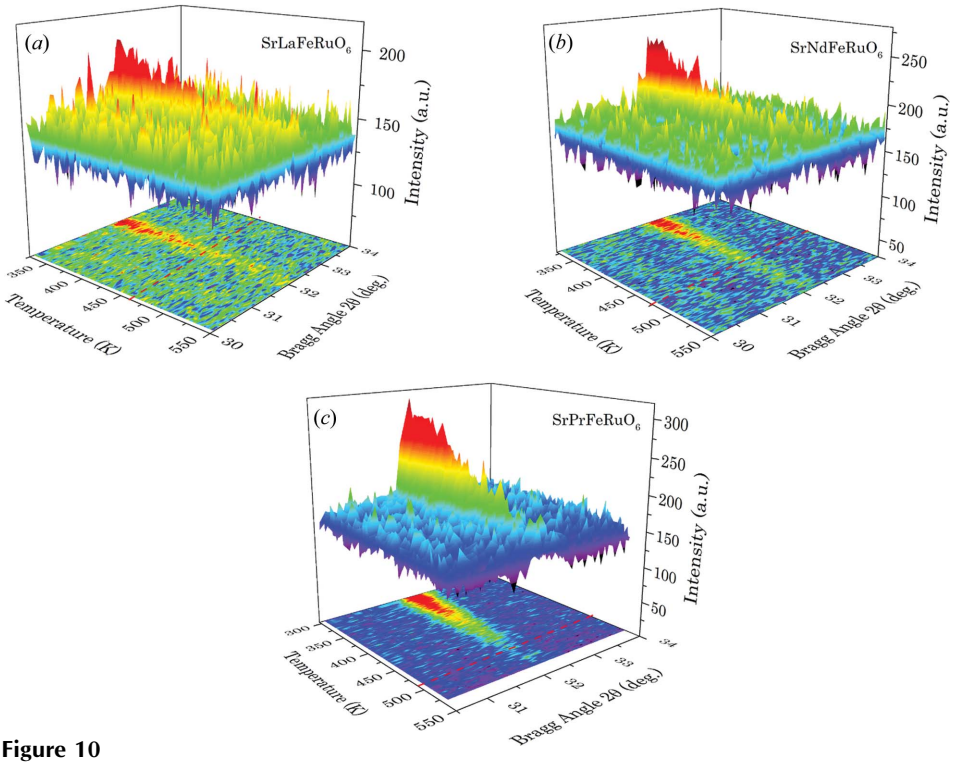

Figure 10
Thermal evolution of the (101) reflection for (*a*) SrLaFeRuO$_6$, (*b*) SrNdFeRuO$_6$ and (*c*) SrPrFeRuO$_6$ collected with λ = 2.52 Å between room temperature and 573 K, in a D1B neutron powder diffractometer.

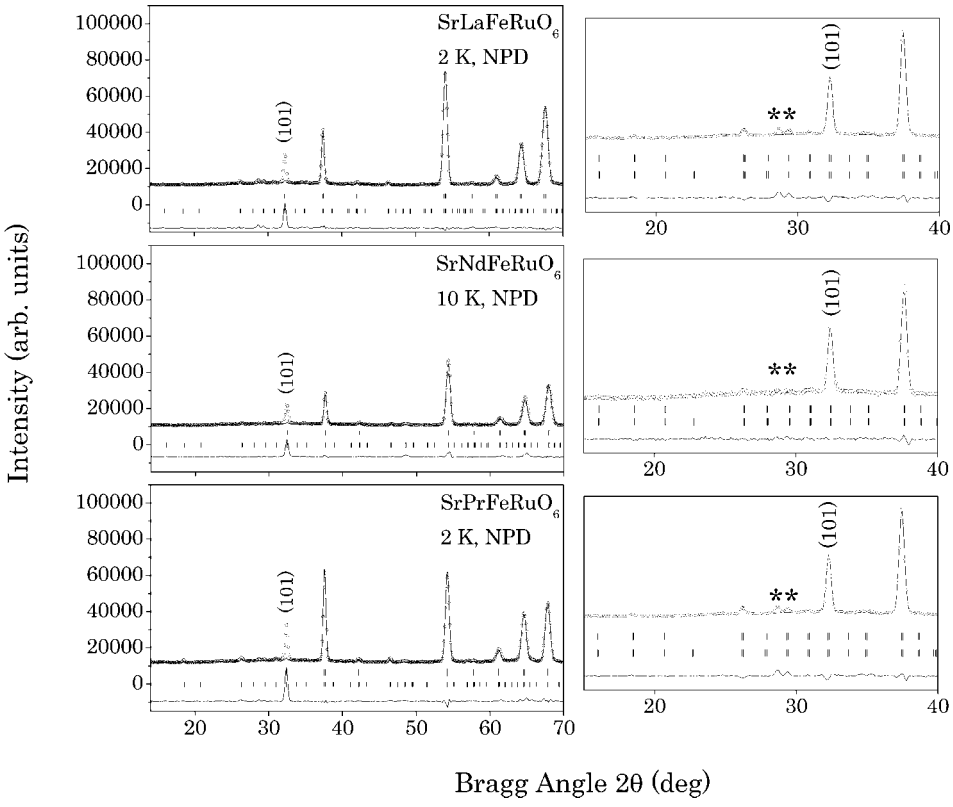

Figure 11
Low-angle region of the neutron powder diffraction patterns collected at low temperature, including the observed intensity (open circles), calculated fit to the data (continuous line) and the difference curve. Tick marks correspond to Bragg peak location, (up) λ = 2.52 Å and (bottom) λ/2 = 1.26 Å. The inset shows the data refinement using the crystal and magnetic model. The upper (lower) marks correspond to the crystal (magnetic) structure using λ = 2.52 Å and λ/2 = 1.26 Å. * La_3RuO_7, Nd_3RuO_7 and Pr_3RuO_7 impurities.

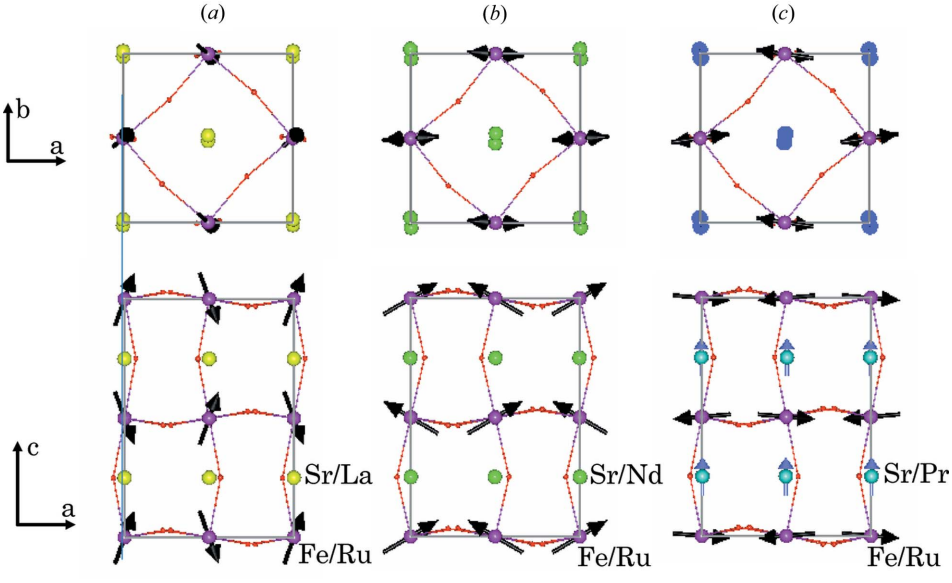

Figure 12
Magnetic structure models: (*a*) $SrLaFeRuO_6$, $3\Gamma_5$ solution; (*b*) $SrNdFeRuO_6$, $3\Gamma_3$ solution; (*c*) $SrPrFeRuO_6$, $3\Gamma_3 \oplus 1\Gamma_3$ solution: Sr/La, yellow balls; Sr/Nd, green balls; Sr/Pr, blue balls, blue arrows; Fe/Ru, purple balls, black arrows; O, red balls.

structure of $SrLaFeRuO_6$, $SrPrFeRuO_6$ and $SrNdFeRuO_6$, the representation analysis described by Bertaut *et al.* (1963) has been performed.

Magnetic ordering for $SrLaFeRuO_6$ and $SrNdFeRuO_6$ is due to Fe^{3+} and Ru^{4+} cations, which share the 4*a* Wyckoff position. Magnetic refinement of the pattern at low temperature was carried out with all the possible models, although the best refinement of the magnetic structure is described by irrep Γ_5 for $SrLaFeRuO_6$ and Γ_3 for $SrNdFeRuO_6$.

$\mathbf{m}_T(4a)$, determined by NPD data refinement (see Fig. 11), is 1.88 (3)μ_B for $SrLaFeRuO_6$ and 2.01 (3)μ_B $SrNdFeRuO_6$; the components along the crystallographic axes are listed in Table 7. This value is far below that expected for the Fe and Ru shared site, 4.5μ_B, S = 5/2 and S = 2, respectively. In Figs. 12(*a*) and (*b*) we illustrate the magnetic structure for $SrLaFeRuO_6$ and $SrNdFeRuO_6$. The models describe a canted-AFM (antiferromagnetic) structure along the *a* axis for the La compound and along *c* for the Nd compound. Table 8 gives structural information at selected temperatures and in Fig. 13 shows the temperature evolution of the magnetic moment in the 4*a* site.

$SrPrFeRuO_6$ shows a more complex magnetic structure, due to the presence of two magnetic sites generated by the Pr ion and Fe/Ru cations. Based on the representation analysis, the only possible irreducible representations are: Γ_1, Γ_3, Γ_5 or Γ_7. The symmetry analysis is not able to discard more models, nor to give information about the phase existing between both magnetic sites. To elucidate the correct magnetic model, irrep Γ_3, NPD data refinement is necessary. The reliability factor for the fitting is R_{mag} = 6.96.

The model for $SrPrFeRuO_6$ is shown in Fig. 12(*c*). The magnetic structure is described by two sites: the spins of the Pr cation in the 4*c* site is strictly FM-ordered along the

Table 8
Structural details of $SrLaFeRuO_6$ obtained at different temperatures from NPD (D1B, ILL) data using the *Pbnm* structural model with R_4^+, M_3^+ and X_5^+ modes refined.

Temperature (K)		2	50	150	200	250
Sr/La	$(x, y, 1/4)$					
	x	0.00 (0)	0.00 (0)	0.00 (0)	0.00 (0)	0.00 (0)
	y	−0.0204 (6)	−0.0215 (5)	−0.0192 (6)	−0.0191 (6)	−0.0186 (6)
	B_{iso} (Å^2)	0.31 (5)	0.26 (5)	0.49 (4)	0.57 (4)	0.69 (5)
Fe/Ru	(0, 1/2, 0)					
	B_{iso} (Å^2)	0.22 (4)	0.19 (4)	0.28 (4)	0.28 (4)	0.32 (4)
	m(Fe/Ru) (μ_B)	1.90 (1)	1.89 (1)	1.70 (1)	1.49 (1)	1.31 (1)
O1	$(x, y, 1/4)$					
	x	−0.0695 (3)	−0.0697 (3)	−0.0680 (3)	−0.0669 (3)	−0.0660 (3)
	y	0.50698	0.50698	0.50698	0.50698	0.50698
	B_{iso} (Å^2)	0.45 (3)	0.42 (3)	0.57 (3)	0.67 (3)	0.81 (3)
O2	x	0.7235 (3)	0.7236 (3)	0.7243 (3)	0.7244 (3)	0.7251 (3)
	y	0.2760 (3)	0.2760 (3)	0.2752 (3)	0.2751 (3)	0.2744 (3)
	z	0.5306 (1)	0.5307 (1)	0.5299 (1)	0.5293 (1)	0.5288 (1)
	B_{iso} (Å^2)	0.45 (3)	0.42 (3)	0.57 (3)	0.67 (3)	0.81 (3)
a (Å)		5.5703 (3)	5.5706 (3)	5.5730 (2)	5.5748 (3)	5.5774 (3)
b (Å)		5.5490 (3)	5.5495 (3)	5.5503 (2)	5.5516 (3)	5.5533 (3)
c (Å)		7.8480 (3)	7.8471 (3)	7.8511 (3)	7.8538 (3)	7.8563 (3)
V (Å^3)		242.58 (2)	242.59 (2)	242.85 (2)	243.07 (2)	243.33 (2)
R_p		0.014	0.014	0.015	0.014	0.015
R_{wp}		0.021	0.022	0.021	0.021	0.021
R_{exp}		0.008	0.008	0.008	0.008	0.008
R_{Bragg}		0.031	0.031	0.033	0.034	0.038
R_{mag}		0.048	0.039	0.061	0.067	0.074

c axis; whereas the magnetic moments on the Fe/Ru ions in the 4*a* site are AFM ordered with a very small canting along the c axis, probably induced by the 4*c*-site magnetic moments. For the Pr-containing compound, the global magnetic moment is strictly ferrimagnetic. However, the small value of the z component for site 4*a* is uncertain. Due to the refinement limitations as a result of a few magnetic peaks and their low intensities there is not enough information to be sure of the sign of the value. Nevertheless, it is reported with a negative sign since it is the refinement result. $\mathbf{m}_{4a}$ for the Pr compound is 1.92 (3)μ_B, and $\mathbf{m}_{4c}$ for Pr 0.63μ_B (Table 7 shows the list of components along the crystallographic axes).

The room-temperature structural information reported for the $SrLaFeRuO_6$ compound by Shaheen *et al.* (2008) is somewhat different from that shown in Table 2. Shaheen *et al.* (2008) conclude from their Mössbauer spectroscopy experiment that their compound does not have any long-range magnetic ordering at room temperature. Nevertheless, during the experiments done to complete this work it became clear that the compound reported here is magnetic at room temperature, and the characterization of the magnetic moment at room temperature has been done (see Table 8). The small differences in lattice parameters and small atomic position variations between the compound presented here and in Shaheen *et al.* (2008) could be the reason to observe long-range magnetic ordering at room temperature in our sample.

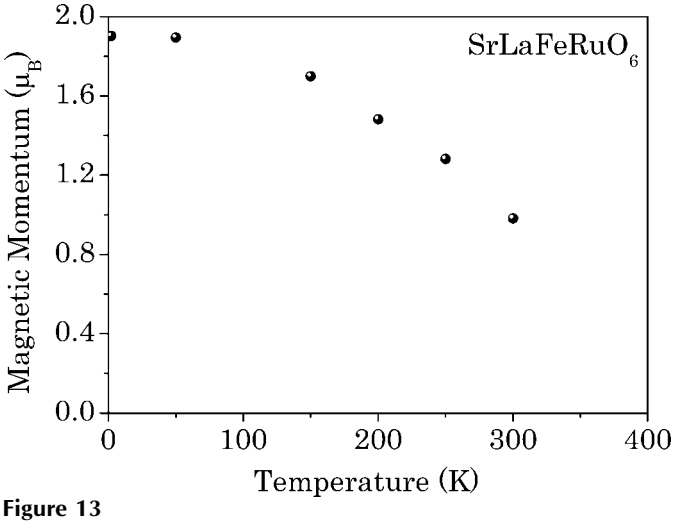

Figure 13
Temperature dependence of $SrLaFeRuO_6$ 4*a*-site Fe/Ru magnetic momentum for the $3\Gamma_5$ solution.

4. Conclusions

The crystal and magnetic structures of $SrLnFeRuO_6$ (*Ln* = La, Pr, Nd) double perovskites have been studied by means of X-ray and neutron powder diffraction techniques. Diffraction experiments show that $SrLnFeRuO_6$ materials have complete chemical disorder of Fe^{3+} and Ru^{4+}, due to small charge and size differences between Fe and Ru cations. All compounds crystallize in the orthorhombic space group *Pbnm*. Analysis of distortion modes shows that the symmetry breaking from the archetype cubic phase to the orthorhombic phase is driven by R_4^+ and M_3^+, in agreement with earlier works (Perez-Mato *et al.*, 2010; Macquart *et al.*, 2010). R_4^+ and M_3^+ distortion mode amplitudes for La, Pr and Nd materials are 0.980 (4) and 0.494 (7), 1.085 (4) and 0.627 (4), and 1.133 (4) and 0.627 (5) Å, respectively.

The temperature-induced structural phase transition was studied for $SrPrFeRuO_6$. NPD pattern refinement suggests the $Pbnm \rightarrow R\bar{3}c$ transition at $\sim$ 1075 K.

The magnetic structure for the three phases is described by the (0,0,0) propagation vector. $SrLaFeRuO_6$ and $SrNdFeRuO_6$ order antiferromagnetically with spin canting along the a and c axis, respectively. $SrPrFeRuO_6$ is more complex as a result of two magnetic sites generated by Pr and

Fe/Ru cations. The global magnetic moment is strictly ferrimagnetic.

This work has been supported by ILL (grant MBR-GL/09-056 and MBR-GL/11-050), the Spanish Ministry of Science and Innovation (project MAT2008-05839) and the European Commission under the 7th Framework Program through the 'Research Infrastructures' action of the 'Capacities' Program, Contract No: CP-CSA_INFRA-2008-1.1.1 Number 226507-NMI3. The authors are grateful to FRMII (exp. 4456), ILL (exp. 5-24-458) and PSI (exp. 20101302) for the beamtime allocation and the instrument local contacts Dr Markus Hoelzel (SPODI, FRMII), Dr Gabriel Cuello (D2B, ILL) and Dr Vladimir Pumjakushin (HRPT, SINQ, PSI) for their kind help and technical assistance.

References

Aroyo, M. I., Kirov, A., Capillas, C., Perez-Mato, J. M. & Wondratschek, H. (2006). *Acta Cryst.* A**62**, 115–128.
Aroyo, M. I., Perez-Mato, J. M., Capillas, C., Kroumova, E., Ivantchev, S., Madariaga, G., Kirov, A. & Wondratsechek, H. (2006). *Z. Kristallogr.* **221**, 15–27.
Bertaut, E. F., Rado, G. & Suhl, H. (1963). *Magnetism*, Vol. III, p. 149. New York, London: Academic Press.
Bos, J. W. G. & Attfield, J. P. (2004). *Chem. Mater.* **16**, 1822–1827.
Brown, I. D. & Altermatt, D. (1985). *Acta Cryst.* B**41**, 244–247.
Faik, A., Igartua, J. M., Gateshki, M. & Cuello, G. J. (2009). *J. Solid State Chem.* **182**, 1717–1725.
Fischer, P., Frey, G., Koch, M., Könnecke, M., Pomjakushin, V., Schefer, J., Thut, R., Schlumpf, N., Bürge, R., Greuter, U., Bondt, S. & Berruyer, E. (2000). *Physica B*, **276–278**, 146–147.
Gateshki, M. & Igartua, J. M. (2003). *Mater. Res. Bull.* **38**, 1893–1900.
Glazer, A. M. (1972). *Acta Cryst.* B**28**, 3384–3392.
Glazer, A. M. (1975). *Acta Cryst.* A**31**, 756–762.
Hoelzel, M., Senyshyn, A., Juenke, N., Boysen, H., Schmahl, W. & Fuess, H. (2012). *Nucl. Instrum. Methods A*, **667**, 32–37.
Hong, K., Choi, Y., Kwon, Y., Jung, D., Lee, J., Shim, H. & Lee, C. (2000). *J. Solid State Chem.* **150**, 383–390.
Horikubi, T., Mori, T., Nonobe, H. & Kamegashira, N. (1999). *J. Alloys Compd.* **289**, 42–47.
Howard, C. J. & Stokes, H. T. (1998). *Acta Cryst.* B**54**, 782–789.
Howard, C. J. & Stokes, H. T. (2005). *Acta Cryst.* A**61**, 93–111.
Iturbe-Zabalo, E., Faik, A., Larrañaga, A., Hoelzel, M. J. C. G. & Igartua, J. M. (2013). *J. Solid State Chem.* **198**, 24–38.
Iturbe-Zabalo, E., Igartua, J. M., Aatiq, A. & Pomjakushin, V. (2013). *J. Mol. Struct.* **1034**, 134–143.
Kim, S. H. & Battle, P. D. (1995). *J. Solid State Chem.* **114**, 174–183.
Kobayashi, K. I., Kimura, T., Sawada, H., Terakura, K. & Tokura, Y. (2006). *Nature*, **395**, 677–680.
Kobayashi, K. I., Kimura, T., Tomioka, Y., Sawada, H. & Terakura, K. (1999). *Phys. Rev. B*, **59**, 11159–11162.
Macquart, R. B., Kennedy, B. J. & Avdeev, M. (2010). *J. Solid State Chem.* **183**, 2400–2405.
Orobengoa, D., Capillas, C., Aroyo, M. I. & Perez-Mato, J. M. (2009). *J. Appl. Cryst.* **42**, 820–833.
Perez-Mato, J. M., Orobengoa, D. & Aroyo, M. I. (2010). *Acta Cryst.* A**66**, 558–590.
Rietveld, H. M. (1969). *J. Appl. Cryst.* **2**, 65–71.
Rodríguez-Carvajal, J. (1993). *Physica B*, **192**, 55.
Shaheen, R., Bashir, J., Nasir, M. K., Rauf, R. & Siddique, M. (2008). *Solid State Sci.* **10**, 1408–1411.
Shannon, R. D. (1976). *Acta Cryst.* A**32**, 751–767.
Wills, A. S. (2000). *Physica B*, **276**, 680.
Woodward, P. M. (1997). *Acta Cryst.* B**53**, 32–43.
Woodward, P., Goldberger, J., Stoltzfus, M., Eng, H., Ricciardo, R., Santhosh, P., Karen, P. & Moodenbaugh, A. (2008). *J. Am. Ceram. Soc.* **91**, 1796–1806.